Structural Engineering and Mechanics, *Vol. 73, No. 1 (2020) 65-73*
DOI: https://doi.org/10.12989/sem.2020.73.1.065

An effective locally-defined time marching procedure for structural dynamics

Tales Vieira Sofiste[1a], Delfim Soares Jr[*2] and Webe João Mansur[1b]

[1]*Civil Engineering Department, COPPE, Federal University of Rio de Janeiro. Modeling Methods in Engineering and Geophysics Laboratory - LAMEMO, Rio de Janeiro, RJ, Brazil*
[2]*Structural Engineering Department, Federal University of Juiz de Fora, Juiz de Fora, MG, Brazil*

(Received November 12, 2018, Revised July 18, 2019, Accepted August 27, 2019)

Abstract. The present work describes a new time marching procedure for structural dynamics analyses. In this novel technique, time integration parameters are automatically evaluated according to the properties of the model. Such parameters are locally defined, allowing the user to input a numerical dissipation property for each element, which defines the amount of numerical dissipation to be introduced. Since the integration parameters are locally defined as a function of the structural element itself, the time marching technique adapts according to the model, providing enhanced accuracy. The new methodology is based on displacement-velocity relations and no computation of accelerations is required. Furthermore, the method is second order accurate, it has guaranteed stability, it is truly self-starting and it allows highly controllable algorithm dissipation in the higher modes. Numerical results are presented and compared to those provided by the Newmark and the Bathe methods, illustrating the good performance of the new time marching procedure.

Keywords: structural dynamics; time marching; adaptive analyses; local parameters; controllable dissipation

1. Introduction

Numerical methods are important tools for solution of complex problems in various branches of science and engineering. In structural dynamics problems, numerical methods are employed in order to obtain stresses, strains or displacements of a system subject to an arbitrary load or initial condition. In this context, the finite element method may be used for the spatial discretization, whereas the dynamic response may be obtained through two main approaches. The first approach applies the mode superposition method, and the final response is obtained as a sum of respective vibration modes. In the second approach, referred as direct integration, no transformation of the equations into a different form is applied (Bathe 1996) and therefore the response is directly computed through time-marching or step-by-step methods. The literature reports many classical implicit (Houbolt 1950, Newmark 1959, Park 1975, Hilber *et al.* 1977, Wood *et al.* 1980, Mohammadzadeh *et al.* 2017) and explicit (Tamma and Namburu 1990, Chung and Lee 1994, Hulbert and Chung 1996, Shojaee *et al.* 2011, Noh and Bathe 2013, Wen *et al.* 2014, Soares 2016) methods for structural dynamics analysis. For a comprehensive review, see Dokainish and Subbaraj (1989), Subbaraj and Dokainish (1989), Tamma *et al.* (2000) and Fung (2003).

For structural dynamics problems, numerical damping may become an important feature of time-marching techniques, since the spatial discretization introduces spurious high frequencies modes into the analysis. Thus, controllable dissipation should suppress the participation of high frequencies modes without interfere in the low frequencies modes, which properly generate the solution response. In this context, several methods have been proposed (Bathe and Baig 2005, Yin 2013, Chang 2014, Chang *et al.* 2015, Shojaee *et al.* 2015, Soares 2011,2017, Rezaiee-Pajand and Karimi-Rad 2018) in order to introduce numerical dissipation of spurious high frequencies. The classical Newmark method is widely used and accepted both in the practical engineering and scientific community, however, it is only first order accurate when numerical damping is activated.

Following the framework presented by Soares (2015, 2017), a novel implicit time integration procedure is proposed here. In this new method, the user is able to select which elements are going to receive numerical dissipation and which are not. In order to do so, the user provides an extra property (as the physical properties of the model are provided) for each element of the spatial discretization (the so-called numerical dissipation parameter, which will be referred here as a^e), enabling controllable, locally-defined, numerical dissipation to be considered into the analyses.

Considering globally (Soares 2016, Soares and Großeholz 2018) and locally (Soares 2017, 2019a, 2019b, 2019c) defined adaptive time-marching procedures is not new, regarding structural dynamics and wave propagation analysis, as well as other transient applications (Soares and Wrobel 2019). However, in this work, a novel methodology is proposed, in which the user locally defines the properties of the time-solution procedure as he/she defines the standard properties of the elements that are spatially discretizing the model. Thus, here, the user is able to select

∗Corresponding author, Professor
E-mail: delfim.soares@ufjf.edu.br
[a] M.Sc.
[b] Ph.D.

ISSN: 1225-4568 (Print), 1598-6217 (Online)

in which elements of the model numerical damping is to be considered (as well as its intensity) and the technique is then adaptively developed according to this definition.

2. Governing equations and the new time marching procedure

The governing system of equations that describes a dynamic model is given by (Clough and Penzien 1995):

$$\boldsymbol{M}\ddot{\boldsymbol{U}}(t) + \boldsymbol{C}\dot{\boldsymbol{U}}(t) + \boldsymbol{K}\boldsymbol{U}(t) = \boldsymbol{F}(t), \tag{1}$$

where $\boldsymbol{F}(t)$ stands for the load vector; $\boldsymbol{M}$, $\boldsymbol{C}$ and $\boldsymbol{K}$ stand for mass, damping and stiffness matrices, respectively, and $\boldsymbol{U}(t)$, $\dot{\boldsymbol{U}}(t)$ and $\ddot{\boldsymbol{U}}(t)$ are displacement, velocity and acceleration vectors, respectively. The initial conditions of the model are given by:

$$\boldsymbol{U}^0 = \boldsymbol{U}(0), \tag{2a}$$

$$\dot{\boldsymbol{U}}^0 = \dot{\boldsymbol{U}}(0), \tag{2b}$$

where $\boldsymbol{U}^0$ and $\dot{\boldsymbol{U}}^0$ stand for initial displacement and initial velocity vectors, respectively.

Considering a constant time-step Δt and the integration of Eq. (1) with respect to time, at the element level (represented with subscript e) one may write:

$$\begin{aligned}\boldsymbol{M}_e \int_{\tau-\frac{\Delta t}{2}}^{\tau+\frac{\Delta t}{2}} \ddot{\boldsymbol{U}}_e(t)\,dt + \boldsymbol{C}_e \int_{\tau-\frac{\Delta t}{2}}^{\tau+\frac{\Delta t}{2}} \dot{\boldsymbol{U}}_e(t)\,dt + \\ \boldsymbol{K}_e \int_{\tau-\frac{\Delta t}{2}}^{\tau+\frac{\Delta t}{2}} \boldsymbol{U}_e(t)\,dt = \int_{\tau-\frac{\Delta t}{2}}^{\tau+\frac{\Delta t}{2}} \boldsymbol{F}_e(t)\,dt.\end{aligned} \tag{3}$$

The integrals in the left-hand side of Eq. (3) may be calculated as (Soares 2015):

$$\int_{\tau-\frac{\Delta t}{2}}^{\tau+\frac{\Delta t}{2}} \ddot{\boldsymbol{U}}_e(t)\,dt = \dot{\boldsymbol{U}}_e^{n+1} - \dot{\boldsymbol{U}}_e^{n}, \tag{4a}$$

$$\int_{\tau-\frac{\Delta t}{2}}^{\tau+\frac{\Delta t}{2}} \dot{\boldsymbol{U}}_e(t)\,dt = \boldsymbol{U}_e^{n+1} - \boldsymbol{U}_e^{n}, \tag{4b}$$

$$\int_{\tau-\frac{\Delta t}{2}}^{\tau+\frac{\Delta t}{2}} \boldsymbol{U}_e(t)\,dt = \Delta t\boldsymbol{U}_e^{n} + \tfrac{1}{2}\alpha_e^n \Delta t^2 \dot{\boldsymbol{U}}_e^{n} + \tfrac{1}{2}\gamma_e^n \Delta t^2 \dot{\boldsymbol{U}}_e^{n+1}, \tag{4c}$$

where α_e^n and γ_e^n are the parameters of the new method, computed for each element at each time step, and the superscripts n and $n+1$ represent the time step of the variables. The displacement $\boldsymbol{U}^{n+1}$ can be defined as:

$$\boldsymbol{U}^{n+1} = \boldsymbol{U}^{n} + \frac{1}{2}\Delta t\left(\dot{\boldsymbol{U}}^{n} + \dot{\boldsymbol{U}}^{n+1}\right). \tag{5}$$

Considering Eqs. (4)-(5), Eq. (3) may be rewritten as the simple following recursive relation:

$$\begin{aligned}\left(\boldsymbol{M}_e + \tfrac{1}{2}\Delta t\boldsymbol{C}_e + \tfrac{1}{2}\gamma_e^n \Delta t^2 \boldsymbol{K}_e\right)\dot{\boldsymbol{U}}_e^{n+1} = \int_{\tau-\frac{\Delta t}{2}}^{\tau+\frac{\Delta t}{2}} \boldsymbol{F}_e(t)\,dt + \\ \boldsymbol{M}_e\dot{\boldsymbol{U}}_e^{n} - \tfrac{1}{2}\Delta t\boldsymbol{C}_e\dot{\boldsymbol{U}}_e^{n} - \boldsymbol{K}_e\left(\Delta t\boldsymbol{U}_e^{n} + \tfrac{1}{2}\alpha_e^n \Delta t^2 \dot{\boldsymbol{U}}_e^{n}\right).\end{aligned} \tag{6}$$

Thus, after assemblage is carried out, it is possible to compute velocities following Eq. (6) and then displacements may be evaluated following Eq. (5). The first important feature of the proposed technique is that Eqs. (5)-(6) are based only on displacements and velocities relations and therefore no computation of accelerations is required. Hence, the new method is truly self-starting, eliminating any need of initial procedures, such as computation of initial accelerations or the computation of multistep initial values.

The integration parameters α_e^n and γ_e^n are locally defined and computed based on the properties of the element, the time-step Δt and the value of the numerical dissipative property a_e. Since only linear analysis are going to be considered in this paper, these parameters remain the same along time (*i.e.*, $\alpha_e^n = \alpha_e$ and $\gamma_e^n = \gamma_e$). The value of the numerical dissipative property defines the amount of numerical damping that will be introduced in each element. The strategy of the present method is to let the user select the structural element in which numerical dissipation is to be activated. In order to achieve this, the user will provide the numerical dissipation property a_e to each element. Wherever numerical dissipation is to be considered, $a^e > 0$ will be adopted, otherwise $a_e = 0$ will be provided. Then, if $a_e = 0$, the following definition for the time integration parameters are considered:

$$\gamma_e = \tfrac{1}{2}\tanh\left(\tfrac{1}{4}\omega_e^{max}\Delta t\right), \tag{7a}$$

$$\alpha_e = 1 - \gamma_e. \tag{7b}$$

Otherwise, if $a_e > 0$, γ_e and α_e are given by:

$$\gamma_e = \tfrac{1}{2} + \tfrac{3}{2}\tanh(a_e\omega_e^{max}\Delta t), \tag{8a}$$

$$\alpha_e = 2(2\gamma_e)^{\frac{1}{2}} - \gamma_e - 1, \tag{8b}$$

where ω_e^{max} stands for the maximum natural frequency of the element, computed as the square root of the highest eigenvalue of the element, considering the generalized eigenvalue problem of the local matrices $\boldsymbol{M}_e$ and $\boldsymbol{K}_e$:

$$\boldsymbol{K}_e\phi_e = \omega_e^2\boldsymbol{M}_e\phi_e. \tag{9}$$

Eq. (7) is proposed in order to obtain reduced period elongation errors (for further details, see Soares (2017)). It is important to highlight that Eq. (8) converges to $\gamma_e = 2$ and $\alpha_e = 1$ for large a_e values. In this case, maximum numerical dissipation is introduced in the element. In the next section, the properties of the proposed technique are presented and further discussed.

3. Properties of the method

In order to discuss the properties of the proposed technique, the equation of motion of a single degree of freedom model is considered:

$$\ddot{u} + 2\xi\omega\dot{u} + \omega^2 u = 0, \tag{10}$$

where ω and ξ stand for the natural frequency of the model and the damping ratio, respectively. Then, taking into

account Eq. (10) and the proposed method, the following recursive relation can be written:

$$\begin{bmatrix} u^{n+1} \\ \dot{u}^{n+1} \end{bmatrix} = \begin{bmatrix} A_{11} & A_{12} \\ A_{21} & A_{22} \end{bmatrix} \begin{bmatrix} u^{n} \\ \dot{u}^{n} \end{bmatrix} = \boldsymbol{A} \begin{bmatrix} u^{n} \\ \dot{u}^{n} \end{bmatrix}, \tag{11}$$

where $\boldsymbol{A}$ stands for the amplification matrix, whose terms can be described as:

$$A_{11} = \frac{1+\xi\omega\Delta t+\frac{1}{2}(\gamma-1)\omega^2\Delta t^2}{1+\xi\omega\Delta t+\frac{1}{2}\gamma\omega^2\Delta t^2}, \tag{12a}$$

$$A_{12} = \frac{[1+\frac{1}{4}(\gamma-\alpha)\omega^2\Delta t^2]\Delta t}{1+\xi\omega\Delta t+\frac{1}{2}\gamma\omega^2\Delta t^2}, \tag{12b}$$

$$A_{21} = \frac{[-\omega^2\Delta t^2](\frac{1}{\Delta t})}{1+\xi\omega\Delta t+\frac{1}{2}\gamma\omega^2\Delta t^2}, \tag{12c}$$

$$A_{22} = \frac{1-\xi\omega\Delta t-\frac{1}{2}\alpha\omega^2\Delta t^2}{1+\xi\omega\Delta t+\frac{1}{2}\gamma\omega^2\Delta t^2}. \tag{12d}$$

3.1 Convergence

The expansion in Taylor series of the analytical amplification matrix is given by:

$$A_{11}^a = 1 - \tfrac{1}{2}\omega^2\Delta t^2 + \tfrac{1}{3}\xi\omega^3\Delta t^3 + O(\Delta t^4), \tag{13a}$$

$$A_{12}^a = \Delta t - \xi\omega\Delta t^2 - \tfrac{1}{6}(1-4\xi^2)\omega^2\Delta t^3 + O(\Delta t^4), \tag{13b}$$

$$A_{21}^a = -\omega^2\Delta t + \xi\omega^3\Delta t^2 + \tfrac{1}{6}(1-4\xi^2)\omega^4\Delta t^3 + O(\Delta t^4), \tag{13c}$$

$$A_{22}^a = 1 - 2\xi\omega\Delta t - (\tfrac{1}{2}-2\xi^2)\omega^2\Delta t^2 + \tfrac{2}{3}(\xi - 2\xi^3)\omega^3\Delta t^3 + O(\Delta t^4). \tag{13d}$$

On the other hand, the expansion in Taylor series of the amplification matrix of the proposed method is given by:

$$A_{11} = 1 - \tfrac{1}{2}\omega^2\Delta t^2 + \tfrac{1}{2}\xi\omega^3\Delta t^3 + O(\Delta t^4), \tag{14a}$$

$$A_{12} = \Delta t - \xi\omega\Delta t^2 - (\tfrac{1}{4}(\gamma+\alpha)-\xi^2)\omega^2\Delta t^3 + O(\Delta t^4), \tag{14b}$$

$$A_{21} = -\omega^2\Delta t + \xi\omega^3\Delta t^2 + (\tfrac{1}{2}\gamma-\xi^2)\omega^4\Delta t^3 + O(\Delta t^4), \tag{14c}$$

$$A_{22} = 1 - 2\xi\omega\Delta t - (\tfrac{1}{2}(\gamma+\alpha)-2\xi^2)\omega^2\Delta t^2 + (\tfrac{1}{2}(3\gamma+\alpha)\xi - 2\xi^3)\omega^3\Delta t^3 + O(\Delta t^4). \tag{14d}$$

By comparing the analytical amplification matrix expansion in Taylor series (Eq. (13)) with the amplification matrix expansion in Taylor series of the proposed method (Eq. (14)), one may observe that the new procedure is second order accurate when $\gamma + \alpha = 1$, which is always the case when $a_e = 0$, as Eq. (7(b)) indicates.

The expansion in Taylor series of the amplification matrix of the proposed method when the numerical damping is activated ($a_e > 0$) – *i.e.,* considering Eqs. (8) – is given by:

$$A_{11} = 1 - \tfrac{1}{2}\omega^2\Delta t^2 + \tfrac{1}{2}\xi\omega^3\Delta t^3 + O(\Delta t^4), \tag{15a}$$

$$A_{12} = \Delta t - \xi\omega\Delta t^2 - (\tfrac{1}{4}-\xi^2)\omega^2\Delta t^3 + O(\Delta t^4), \tag{15b}$$

$$A_{21} = -\omega^2\Delta t + \xi\omega^3\Delta t^2 + (\tfrac{1}{4}-\xi^2)\omega^4\Delta t^3 + O(\Delta t^4), \tag{15c}$$

$$A_{22} = 1 - 2\xi\omega\Delta t - (\tfrac{1}{2}-2\xi^2)\omega^2\Delta t^2 + (-\tfrac{3}{2}a^e\omega_e^{max}\omega^2 + (\xi - 2\xi^3)\omega^3)\Delta t^3 + O(\Delta t^4), \tag{15d}$$

which, by comparing with the analytical amplification matrix expansion in Taylor series, indicates that the method is also second order accurate when numerical dissipation is inserted.

It is important to highlight that the numerical dissipation is locally defined considering the proposed technique. As so, the user may select in which elements numerical damping is to be activated. Thus, in opposite to standard methods, here, numerical damping may be locally defined, allowing parts of the global model to be analyzed considering different intensities of numerical damping. As a consequence, numerical dissipation can be introduced just at some parts of the system, enabling more accurate computations.

3.2 Stability

A method is considered stable when matrix $\boldsymbol{A}$ does not amplify errors as time-stepping advances in time. The conditions required in order to assure stability are (Hughes 1987): (i) the spectral radius of matrix $\boldsymbol{A}$ is less or equal to one ($\rho(\boldsymbol{A}) \leq 1$); (ii) eigenvalues of $\boldsymbol{A}$ of multiplicity greater than one are strictly less than one in modulus.

The spectral radius of $\boldsymbol{A}$ is defined as the maximum absolute eigenvalue of $\boldsymbol{A}$. The eigenvalues of the amplification matrix of the proposed method are given by:

$$\lambda_{1,2}(\mathbf{A}) = A_1 \pm (A_1^2 - A_2)^{\frac{1}{2}}, \tag{16}$$

where A_1 is the half trace of the matrix $\boldsymbol{A}$:

$$A_1 = \frac{1+\frac{1}{4}(-\gamma-\alpha-1)\Omega^2}{1+\xi\Omega+\frac{1}{2}\gamma\Omega^2}, \tag{17}$$

and A_2 is the determinant of matrix $\boldsymbol{A}$:

$$A_2 = \frac{1-\xi\Omega+\frac{1}{2}(1-\alpha)\Omega^2}{1+\xi\Omega+\frac{1}{2}\gamma\Omega^2}, \tag{18}$$

where Ω is the sample frequency, defined as:

$$\Omega = \omega\Delta t. \tag{19}$$

The spectral radius behavior of matrix $\boldsymbol{A}$ demonstrates that the method may be unconditionally stable, conditionally stable or unconditionally unstable, according to the values computed for the time integration parameters γ_e and α_e. Those regions of stability are depicted in Fig. 1.

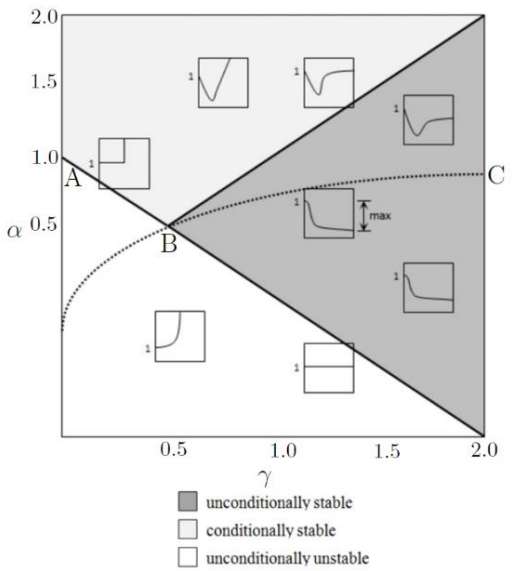

Fig. 1 Spectral radius behavior and regions of stability for the $\alpha - \gamma$ plane

As one may observe, when $a_e = 0$ is adopted, the method is located in the line *AB*, which is a conditionally stable region, on the border of the unconditionally unstable domain. Point *A* basically replicates the Central Difference Method ($\gamma_e = 0$ and $\alpha_e = 1$), and point *B* corresponds to the Trapezoidal Rule ($\gamma_e = 0.5$ and $\alpha_e = 0.5$). It is important to highlight an important feature of the new method: once the Central Difference Method (CDM) presents negative period elongation and the Trapezoidal Rule (TR) presents positive period elongation, the new method presents lower period elongation errors, since it is located between the CDM and the TR when numerical dissipation is not introduced in the analysis. Thus, the new technique is always more accurate than the Trapezoidal Rule, when $a_e = 0$ is considered.

As it is above described, the method is conditionally stable when numerical dissipation is not activated. In this case, the critical sampling frequency is given by:

$$\Omega_c = 2(\alpha - \gamma)^{\frac{-1}{2}}, \tag{20}$$

which means that the method is stable when $\Omega_c \geq \Omega$, and unstable otherwise. The integration parameters γ_e and a_e are computed (Eqs. (7)) based on the maximum sampling frequency of the element Ω^{max}. Since $\Omega_c > \Omega^{max}$ for any Ω_e^{max}, when Eqs. (7) are considered, stability is assured when numerical damping is not included.

On the other hand, when numerical damping is activated ($a_e > 0$), the method is described by the curve *BC* of Fig. 1 (see Eqs. (8)) and, thus, the method stands as an unconditionally stable technique.

The spectral radii for the proposed technique are depicted in Fig. 2 as function of Ω_e ($\Omega_e = \omega_e^{max}\Delta t$). As one may observe, the spectral radius behavior demonstrates that the method is conditionally stable and that stability is always ensured, because $\Omega_c > \Omega_e$, when numerical damping is neglected (Fig 2(a)); and that the method is unconditionally stable, when numerical damping is activated (Fig. 2(b)).

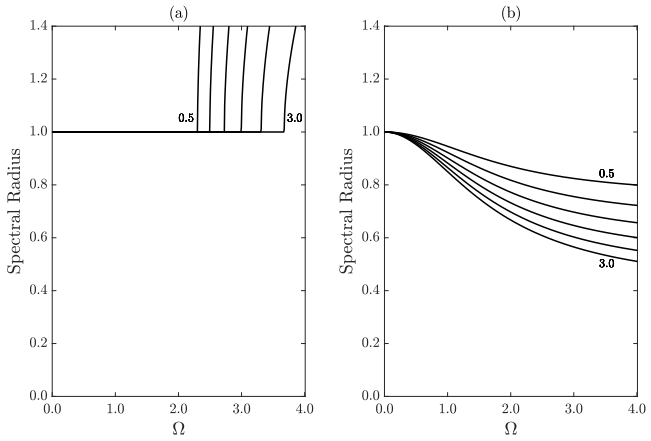

Fig. 2 Spectral radius: $\Omega_e = 0.5; 1.0; 1.5; 2.0; 2.5$ and 3.0. (a) $a_e = 0$; (b) $a_e = 0.1$

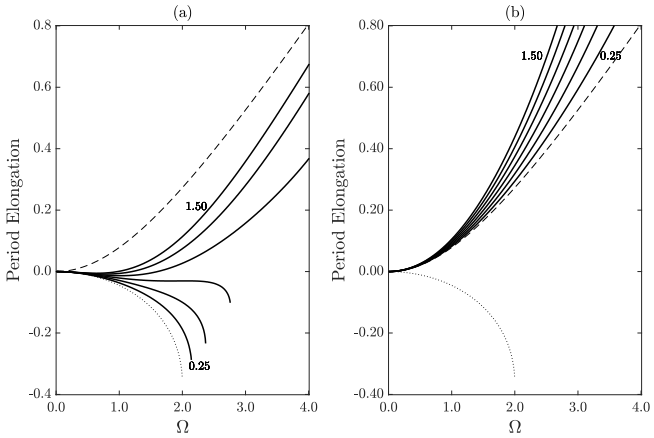

Fig. 3 Period elongation considering $\omega_e^{max}/\omega_e = 0.25; 0.5; 0.75; 1.0; 1.25; 1.5$. (a) $a_e = 0$; (b) $a_e = 0.1$. Dotted lines correspond to the TR and dashed lines correspond to CDM

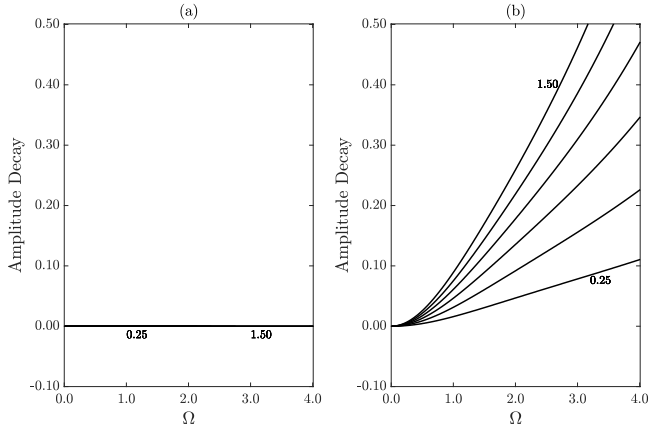

Fig. 4 Amplitude decay considering $\omega_e^{max}/\omega_e = 0.25; 0.5; 0.75; 1.0; 1.25; 1.5$. (a) $a_e = 0$; (b) $a_e = 0.1$

3.3 Accuracy

In order to illustrate the accuracy of the proposed technique, period elongation, amplitude decay and amplitude factor errors are depicted in Figs. 3-5, respectively.

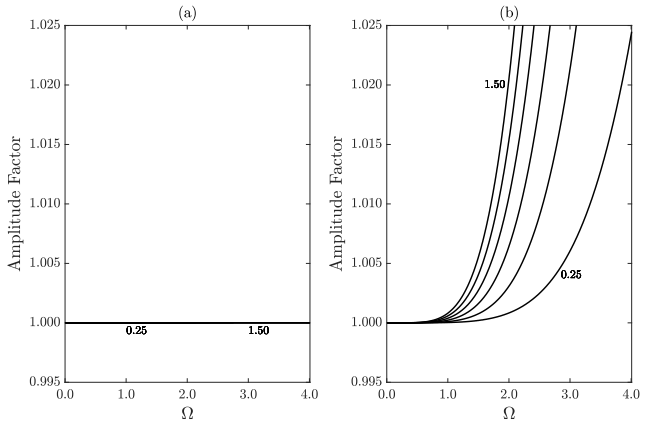

Fig. 5 Amplitude factor considering $\omega_e^{max}/\omega_e = 0.25; 0.5; 0.75; 1.0; 1.25; 1.5$. (a) $a_e = 0$; (b) $a_e = 0.1$

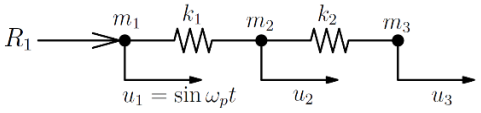

Fig. 6 Three degrees-of-freedom spring model

As one may observe, the period elongation for the Central Difference Method (dotted line) and the Trapezoidal Rule (dashed line) are also presented in Fig. 3. As previously discussed, when numerical damping is neglected, the period elongation errors of the present method are located between those of the CDM and the TR, enabling a very accurate second order methodology.

4. Numerical applications

In this section, three numerical applications are presented in order to illustrate the good performance of the proposed method. First, a three degree-of-freedom spring system is considered, which simulates the stiff and flexible parts of a much more complex structural system. In the sequence, a clamped rod subjected to an initial velocity condition is analyzed. In this case, both homogeneous and heterogeneous media are considered. Finally, a multi degree-of-freedom plane frame is studied. Results are compared to those provided by the Bathe method and the Newmark method. Since the Bathe method is a two-step method (*i.e.*, it requires two systems of equations to be dealt with within each time step), the adopted time step for the Bathe method was also selected twice larger than those of the other methods, in order to evenly compare the computed results in terms of computational costs.

4.1 Spring system

This first numerical application was extracted from Bathe and Noh (2012) (which is further explored in Noh and Bathe 2018, 2019) and consists of a simple three degrees-of-freedom spring model, as shown in Fig. 6.

The governing equations that describes the solution of the three degrees-of-freedom system are:

Table 1 Numerical damping property adopted for each element and correspondent time integration parameters

Element	a_e	γ_e	α_e
1^{st}	1	2	1
2^{nd}	0	0.0461	0.9539

$$\begin{bmatrix} m_1 & 0 & 0 \\ 0 & m_2 & 0 \\ 0 & 0 & m_3 \end{bmatrix} \begin{bmatrix} \ddot{u}_1 \\ \ddot{u}_2 \\ \ddot{u}_3 \end{bmatrix} + \begin{bmatrix} k_1 & -k_1 & 0 \\ -k_1 & k_1 + k_2 & -k_2 \\ 0 & -k_2 & k_2 \end{bmatrix} \begin{bmatrix} u_1 \\ u_2 \\ u_3 \end{bmatrix} = \begin{bmatrix} R_1 \\ 0 \\ 0 \end{bmatrix}, \tag{21}$$

where $k_1 = 10^7$, $k_2 = 1$, $m_1 = 0$ and $m_2 = m_3 = 1$. Null initial conditions are considered at nodes 2 and 3, and the prescribed displacement at node 1 is defined as:

$$u_1 = \sin\, \omega_p t, \tag{22}$$

where $\omega_p t = 1.2$. Since node 1 is subjected to a prescribed displacement, it is possible to rewrite Eq. (21) in terms of the unknown displacements u_2 and u_3:

$$\begin{bmatrix} m_2 & 0 \\ 0 & m_3 \end{bmatrix} \begin{bmatrix} \ddot{u}_2 \\ \ddot{u}_3 \end{bmatrix} + \begin{bmatrix} k_1 + k_2 & -k_2 \\ -k_2 & k_2 \end{bmatrix} \begin{bmatrix} u_2 \\ u_3 \end{bmatrix} = \begin{bmatrix} k_1 u_1 \\ 0 \end{bmatrix}. \tag{23}$$

Then, the reaction R_1 is given by:

$$R_1 = m_1 \ddot{u}_1 + k_1 u_1 - k_1 u_2. \tag{24}$$

In order to compare the obtained results, the same analysis that is carried out by Bathe and Noh (2012) is reproduced here, adopting the time step $\Delta t = 0.2816s$. However, to better illustrate the period elongation and amplitude decay errors of the computed results, a longer period of analysis is considered ($T = 100s$). The strategy here is to adopt $a_e = 1$ (large numerical damping) for the first element of the model and $a_e = 0$ (no numerical damping) for the second element. Table 1 describes the adopted numerical damping properties and time integration parameters, automatically computed according to Eqs. (7)-(8).

In this simple model, the left spring may represent an almost rigid connection while the right spring represents the flexible parts of a much more complex system. Since the Bathe method is a two-step method, results are compared considering it employing the same time-step ($\Delta t = 0.2816s$) that is considered by the other techniques, which is referred here as "Bathe (Δt)", and also considering a twice larger time-step ($\Delta t = 0.5632s$), which is referred here as "Bathe ($2 \times \Delta t$)". Therefore, Bathe ($2 \times \Delta t$) is considered in order to evenly compare the methods in terms of computational costs, while Bathe (Δt) can be considered approximately twice more computationally demanding than the proposed technique (Bathe and Baig 2005). A reference response, obtained by mode superposition and static correction (Bathe 1996, Bathe and Noh 2012) is also presented. Velocities at nodes 2 and 3 are depicted in Figs. 7-8.

As one may observe, the new method and the Bathe method present fast dissipation of artificial high frequencies

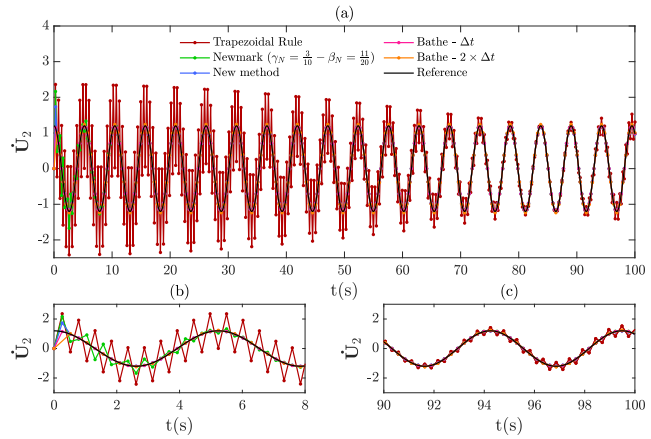

Fig. 7 Velocity at node 2: (a) from 0 to $100s$; (b) from 0 to $8s$; (c) from 90 to $100s$

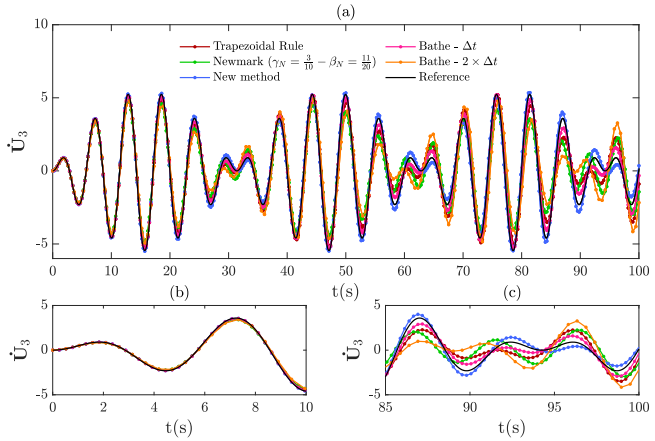

Fig. 8 Velocity at node 3: (a) from 0 to $100s$; (b) from 0 to $10s$; (c) from 85 to $100s$

Table 2 Relative errors for velocities at node 2 and 3

	Trapezoidal Rule	Newmark $\gamma_N = 3/10$ $\beta_N = 11/20$	New method	Bathe (Δt)	Bathe ($2 \times \Delta t$)
$\dot{U}_2$	92.78%	13.56%	8.00%	7.21%	10.64%
$\dot{U}_3$	23.55%	30.52%	9.06%	12.04%	43.59%

(Fig. 7(b)), and the TR provides inappropriate results, since this model presents spurious frequencies due to modelling and such method does not present numerical dissipation. In addition, the new method provides lower period elongation and amplitude decay errors (Fig. 8(c)). Relative errors, evaluated according to Eq. (25), are presented in Table 2.

$$Error = \left[\frac{\sum_{j=1}^{N_t}\left(u(t_j) - u_R(t_j)\right)^2}{\sum_{j=1}^{N_t}\left(u_R(t_j)\right)^2}\right] \times 100\%. \qquad (25)$$

As shown in Table 2, the new method performs very well and presents better results when equivalent computational efforts are considered. It is important to highlight that, for node 3, the performance of the new method is superior even when compared to the "Bathe (Δt)", allowing obtaining better accuracy taking into account considerably reduced computational efforts.

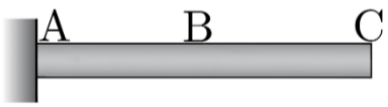

Fig. 9 Sketch of the clamped rod

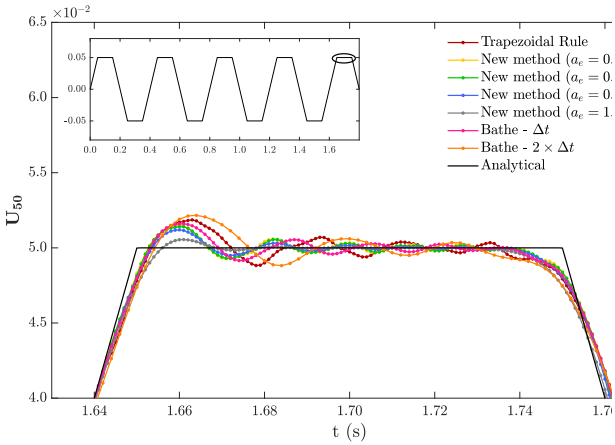

Fig. 10 Time history for the homogeneous rod, at point B

Table 3 Numerical damping property adopted for each element and correspondent time integration parameters

	1^{st} element		Other elements	
	γ_e	α_e	γ_e	α_e
$a_e = 0.00$	0.2311	0.7689	0.2311	0.7689
$a_e = 0.01$	0.5299	0.5291	0.2311	0.7689
$a_e = 0.10$	0.7960	0.7275	0.2311	0.7689
$a_e = 1.00$	1.9460	0.9996	0.2311	0.7689

4.2 Clamped rod

In this second numerical application, a clamped rod is studied. First, a homogeneous rod is considered, and the geometrical and physical properties of the model are: $L = 1\,[m]$ (length), $E = 10^2\,[N/m^2]$ (Young's modulus) and $\rho = 1\,[kg/m^3]$ (mass density). 100 linear finite elements of equal length ($l = 0.01\,[m]$) are employed for the spatial discretization and $\Delta t = 10^{-3}\,[s]$ is adopted. For initial condition, $v_0 = 1\,[m/s]$ (axial velocity) is considered acting over the entire domain.

For this model, the analytical answer for the axial displacement is given by:

$$u_{analytical}(x,t) = \sum_{n=1}^{\infty} \frac{8Lv_0}{(2n-1)^2\pi^2 c} \sin\left(\frac{(2n-1)\pi x}{2L}\right) \sin\left(\frac{(2n-1)\pi ct}{2L}\right), \qquad (26)$$

where c stands for the dilational wave propagation velocity of the medium and $c = 10\,[m/s]$ in this case.

Taking into account the new approach, $a_e > 0$ was adopted only for the first element of the model (located next to the support) and $a_e = 0$ was considered for all other elements. The computed integration parameters are presented in Table 3.

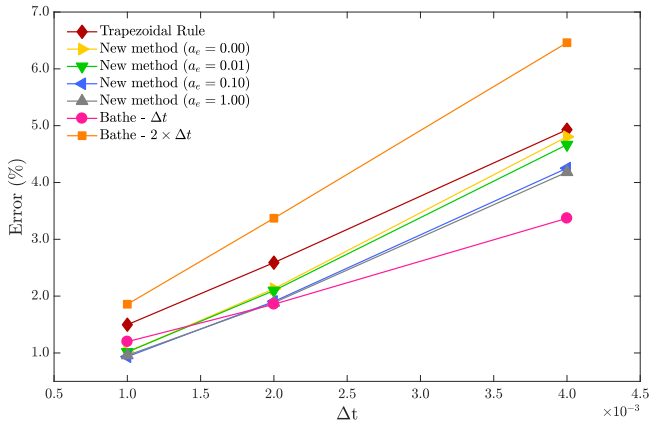

Fig. 11 Relative errors results considering all the 100 finite elements of the spatial discretization

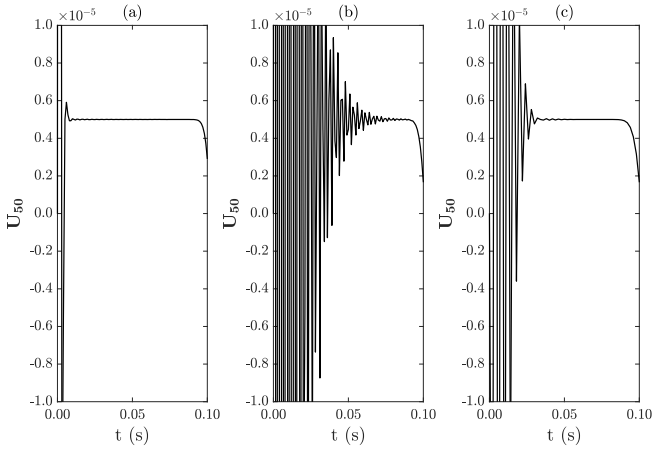

Fig. 12 Time history for the heterogeneous rod at point B (middle of the rod). (a) New method; (b) Bathe - Δt; (c) Bathe - $2 \times \Delta t$

The time history results at the middle of the rod (point B), which corresponds to node 50 of the spatial discretization, is depicted in Fig. 10. In addition, errors results, computed according to Eq. (25), are depicted in Fig. 11, considering several time-steps. In this case, relative errors are calculated considering all the 100 finite elements of the spatial discretization.

As one may observe, even in a homogeneous model, the introduction of numerical damping results in a more accurate response. Considering the same computational costs, the new method demonstrated superior performance compared to the Bathe method ("Bathe - $2 \times \Delta t$") and the Trapezoidal Rule (Fig. 11). For $\Delta t = 10^{-3}\,[s]$ the new method provides better accuracy than "Bathe – Δt", which means that a better response was obtained with almost half of its computational effort.

In order to simulate a rigid connection, a heterogeneous model is studied. It is important to highlight that rigid parts are usually introduced in more complex models in order to simulate constraints. Thus, the Young modulus of half of the rod (point A to point B) is increased to $E_{AB} = 10^6\,[N/m^2]$ and kept the same $E_{BC} = 10^2\,[N/m^2]$ on the other half. In this case, the dilational wave propagation velocities are $c_{AB} = 10^3\,[m/s]$ and $c_{BC} = 10\,[m/s]$.

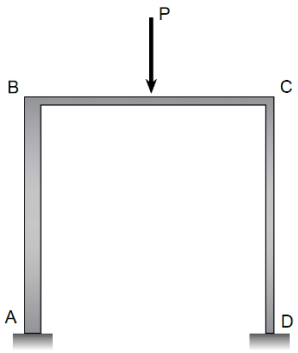

Fig. 13 Plane frame subjected to vertical load

The strategy here is to insert numerical damping into the rigid segment. In order to achieve this, it has been considered $a_e = 1$ from point A to point B and $a_e = 0$ from point B to point C. Then, the time integration parameters are $\gamma_e^{AB} = 2$; $\alpha_e^{AB} = 1$; $\gamma_e^{BC} = 0.2311$ and $\alpha_e^{BC} = 0.7689$. The same time-step ($\Delta t = 10^{-3}\,[s]$) is adopted to analyze the model, considering the new method and the Bathe method.

The displacement time history of node 50 (located at the middle of the rod) is depicted in Fig. 12. As one may observe, the new method presents fast dissipation of artificial high frequencies (Fig. 12(a)) while the Bathe method, considering both the same time-step (Fig. 12(b)) and twice larger time-step (Fig. 12 (c)) presents a poorer performance dissipating the spurious modes of the model.

4.3 Plane frame

The third numerical application is a plane frame subjected to a vertical load, as shown in Fig. 13. The physical and geometrical properties for the model are: $L_{AB} = L_{BC} = L_{CD} = 1\,[m]$ (length of segment), $I_{AB} = I_{BC} = I_{CD} = 10^2\,[m^4]$ (moment of inertia), $\rho_{AB} = \rho_{BC} = \rho_{CD} = 10\,[kg/m^3]$ (mass density). The segment *AB* is considered with higher stiffness than the segments *BC* and *CD*. So, $E_{AB} = 10^{12}\,[N/m^2]$ and $E_{BC} = E_{CD} = 10^7\,[N/m^2]$ (Young modulus).

For the spatial discretization, it has been adopted 151 nodes with 3 degrees of freedom per node (horizontal displacement, vertical displacement and rotation) and hence 150 frame elements with same length. Then, the points *A*, *B*, *C* and *D* correspond to the nodes *1*, *51*, *101* and *151*, respectively. The time-step adopted in the analysis is $\Delta t = 2 \times 10^{-5}\,[s]$ and a vertical unitary load $P = 1\,[N]$ is applied at the middle node of the segment *BC* (node *76*) and kept constant along time. Since there is no analytical response for this model, a reference solution obtained with mode superposition is considered. The modal solution is obtained considering 80 modes of vibration and the Trapezoidal Rule ($\Delta t = 2 \times 10^{-5}\,[s]$) is adopted for the numerical integration of each mode of vibration.

For this model, the stiffer segment *AB* tends to introduce spurious oscillations on the solution. Therefore, taking into account the new method, large numerical dissipation is introduced in the segment *AB* and no numerical dissipation

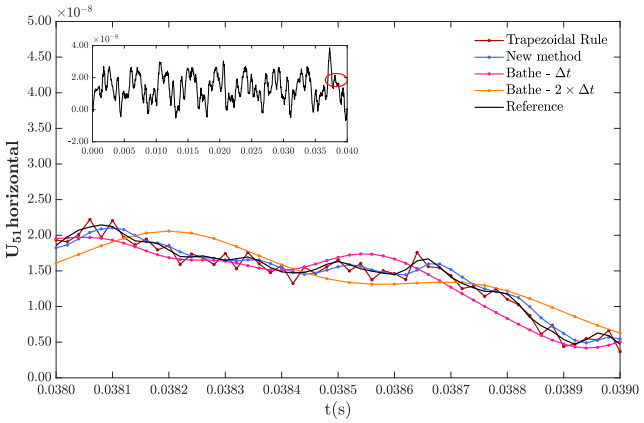

Fig. 14 Horizontal displacement at node *51*

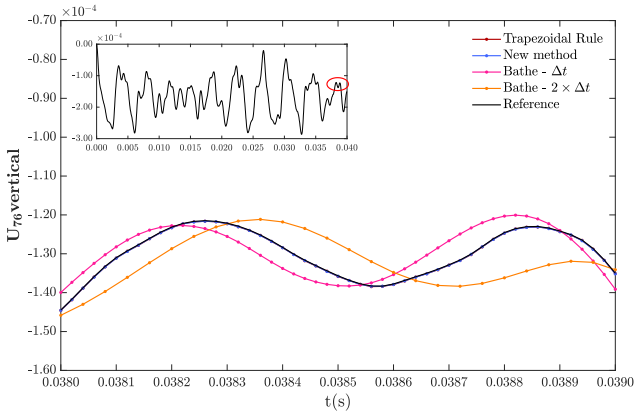

Fig. 15 Vertical displacement at node *76*

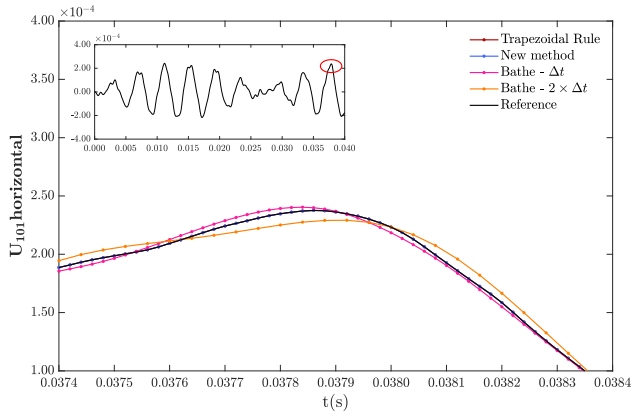

Fig. 16 Horizontal displacement at node *101*

is introduced in the segments *BC* and *CD*. Then, $a_e = 1$ is adopted for the segment *AB*, which leads to $\gamma_e = 2$ and $\alpha_e = 1$ and $a_e = 0$ is adopted for segments *BC* and *CD*, leading to $\gamma_e = 0.5$ and $\alpha_e = 0.5$, which replicates the TR.

In Figs. 14-16, the horizontal displacement at node *51* (point B), vertical displacement at node *76* (middle point of segment *BC*) and horizontal displacement at node *101* (point C) are depicted, respectively.

As one may observe, the Trapezoidal Rule does not dissipate the participation of the artificial modes of vibration while the new method removes the participation of spurious high frequencies (Fig. 14) without deteriorating the response (Figs. 15-16).

5. Conclusions

A novel time marching procedure for structural dynamics analysis is presented in this work. Since the new method is based on displacement and velocities relations, no computation of acceleration is required. As so, the proposed technique is quite simple and efficient in terms of computational effort, once it presents fewer equations to be dealt with in each time step and is truly self-starting, eliminating any kind of initial procedure, such as the computation of initial accelerations or multistep initial values. Furthermore, the new method presents controllable numerical dissipation at element level. Thus, the user can select in which element and in which amount numerical dissipation is going to be introduced in the model. The numerical dissipation property a_e may then be interpreted as a further physical property of the element, such as the moment of inertia, mass density or Young modulus.

As it is discussed along the paper, the method has guaranteed stability and keeps its second order accuracy when numerical dissipation is introduced into the analysis, a characteristic that is not presented in some classical methods, such as the Newmark method. In Section 4 several results are presented, illustrating the good performance of the proposed method. In some cases, the new technique presented better results even when compared to the Bathe method, which is a twice more computationally demanding technique.

Acknowledgments

This study was financed in part by the Coordenação de Aperfeiçoamento de Pessoal de Nível Superior – Brasil (CAPES) – Finance Code 001; CNPq (Conselho Nacional de Desenvolvimento Científico e Tecnológico) and FAPEMIG (Fundação de Amparo à Pesquisa do Estado de Minas Gerais).

References

Bathe, K.J. (1996), *Finite Element Procedures*, Prentice Hall, Upper Saddle River, NJ, USA.

Bathe, K.J. and Baig, M.M.I. (2005), "On a composite implicit time integration procedure for nonlinear dynamics", *Comput. Struct.*, **83**(31-32), 2513-2524. https://doi.org/10.1016/j.compstruc.2005.08.001.

Bathe, K.J. and Noh, G. (2012), "Insight into an implicit time integration scheme for structural dynamics", *Comput. Struct.*, **98**, 1-6. https://doi.org/10.1016/j.compstruc.2012.01.009.

Chang, S-I. (2014), "A family of noniterative integration methods with desired numerical dissipation", *J. Numeric. Method. Eng.*, **100**, 62-86. https://doi.org/10.1002/nme.4720.

Chang, S-Y., Wu, T-H. and Tran, N-C. (2015), "A family of dissipative structure-dependent integration methods", *Struct. Eng. Mech.*, **55**(4), 815-837. https://doi.org/10.12989/sem.2015.55.4.815.

Chung, J. and Lee, J.M. (1994), "A new family of explicit time integration methods for linear and non-linear structural dynamics", *J. Numeric. Method. Eng.*, **37**(23), 3961-3976. https://doi.org/10.1002/nme.1620372303.

Clough, R.W. and Penzien, J. (1995), *Dynamics of Structures*,

Computers and Structures Inc., Berkeley, CA, USA.
Dokainish, M.A. and Subbaraj, K. (1989), "A survey of direct time-integration methods in computational structural dynamics-I. Explicit methods", *Comput. Struct.*, **32**(6), 1371-1386. https://doi.org/10.1016/0045-7949(89)90314-3.
Fung, T.C. (2003), "Numerical dissipation in time-step integration algorithms for structural dynamic analysis", *Progress Struct. Eng. Mater.*, **5**(3), 167-180. https://doi.org/10.1002/pse.149.
Hilber, H.M., Hughes, T.J.R and Taylor, R.L. (1977), "Improved numerical dissipation for time integration algorithms in structural dynamics", *Earthq. Eng. Struct. Dynam.*, **5**(3), 283-292. https://doi.org/10.1002/eqe.4290050306.
Houbolt, J.C. (1950), "A recurrence matrix solution for the dynamic response of elastic aircraft", *J. Aeronautic. Sci.*, **17**(9), 540-550. https://doi.org/10.2514/8.1722.
Hughes, T.J.R. (1987), *The Finite Element Method: Linear Static and Dynamic Finite Element Analysis*, Prentice-Hall, Englewood Cliffs, NJ, USA.
Hulbert, G.M. and Chung, J. (1996), "Explicit time integration algorithms for structural dynamics with optimal numerical dissipation", *Comput. Method. Appl. Mech. Eng.*, **137**(2), 175-188. https://doi.org/10.1016/S0045-7825(96)01036-5.
Mohammadzadeh, S., Ghassemieh, M. and Park, Y. (2017), "Extended implicit integration process by utilizing nonlinear dynamics in finite element", *Struct. Eng. Mech.,* **64**(4), 495-504. https://doi.org/10.12989/sem.2017.6.4.495.
Newmark, N.M. (1959), "A method of computation for structural dynamics", *J. Eng. Mech. Division*, **85**(3), 67-94.
Noh, G. and Bathe, K.J. (2013), "An explicit time integration scheme for the analysis of wave propagations", *Comput. Struct.*, **129**, 178-193. https://doi.org/10.1016/j.compstruc.2013.06.007.
Noh, G. and Bathe, K.J. (2018), "Further insights into an implicit time integration scheme for structural dynamics", *Comput. Struct.*, **202**, 15-24. https://doi.org/10.1016/j.compstruc.2018.02.007.
Noh, G. and Bathe, K.J. (2019), "The Bathe time integration method with controllable spectral radius: The ρ_∞-Bathe method", *Comput. Struct.*, **212**, 299-310. https://doi.org/10.1016/j.compstruc.2018.11.001.
Park, K.C. (1975), "An improved stiffly stable method for direct integration of nonlinear structural dynamic equations", *J. Appl. Mech.*, **42**(2), 464-470.
Rezaiee-Pajand, M. and Karimi-Rad, M. (2018), "A family of second-order fully explicit time integration schemes", *Comput. Appl. Math.*, **37**(3), 3431-3454. https://doi.org/ 10.1007/s40314-017-0520-3.
Shojaee, S., Rostami, S. and Moeinadini, A. (2011), "The numerical solution of dynamic response of SDOF systems using cubic B-spline polynomial functions", *Struct. Eng. Mech.*, **38**(2), 211-229. https://doi.org/10.12989/sem.2011.38.2.211.
Shojaee, S., Rostami, S. and Abbasi, A. (2015), "An unconditionally stable implicit time integration algorithm: modified quartic B-spline method", *Comput. Struct.*, **153**, 98-111. https://doi.org/10.1016/j.compstruc.2015.02.030.
Soares, D. (2011), "A new family of time marching procedures based on Green's function matrices", *Comput. Struct.*, **89**(1-2), 266-276. https://doi.org/10.1016/j.compstruc.2010.10.011.
Soares, D. (2015), "A simple and effective new family of time marching procedures for dynamics", *Comput. Method. Appl. Mech. Eng.*, **283**, 1138-1166. https://doi.org/10.1016/j.cma.2014.08.007.
Soares, D. (2016), "A novel family of explicit time marching techniques for structural dynamics and wave propagation models", *Comput. Method. Appl. Mech. Eng.*, **311**(3), 838-855. https://doi.org/10.1016/j.cma.2016.09.021.
Soares, D. (2017), "A simple and effective single-step time marching technique based on adaptive time integrators", *J. Numeric. Method. Eng.*, **109**(9), 1344-1368. https://doi.org/10.1002/nme.5329.
Soares Jr, D. and Großeholz, G. (2018), "Nonlinear structural dynamic analysis by a stabilized central difference method", *Eng. Struct.*, **173**, 383-392. https://doi.org/10.1016/j.engstruct.2018.06.115.
Soares Jr, D. (2019a), "A locally stabilized central difference method", *Finite Element. Anal. Design*, **155**, 1-10. https://doi.org/10.1016/j.finel.2018.12.001.
Soares Jr, D. (2019b), "An adaptive semi-explicit/explicit time marching technique for nonlinear dynamics", *Comput. Method. Appl. Mech. Eng.*, **354**(1), 637-662. https://doi.org/10.1016/j.cma.2019.05.040.
Soares Jr, D. (2019c), "A model/solution-adaptive explicit-implicit time-marching technique for wave propagation analysis", *J. Numeric. Method. Eng.*, **119**(7), 590-617. https://doi.org/10.1002/nme.6064.
Soares Jr, D. and Wrobel, L.C. (2019), "A locally stabilized explicit approach for nonlinear heat conduction analysis", *Comput. Struct.*, **214**, 40-47. https://doi.org/10.1016/j.compstruc.2019.01.004.
Subbaraj, K. and Dokainish, M.A. (1989), "A survey of direct time-integration methods in computational structural dynamics-II. Implicit methods", *Comput. Struct.*, **32**(6), 1387-1401. https://doi.org/10.1016/0045-7949(89)90315-5.
Tamma, K.K. and Namburu, R.R. (1990), "A robust self-starting explicit computational methodology for structural dynamic applications: architecture and representations", *J. Numeric. Method. Eng.*, **29**(7), 1441-1454. https://doi.org/10.1002/nme.1620290705.
Tamma, K.K., Zhou, X. and Sha, D. (2000), "The time dimension: a theory towards the evolution, classification, characterization and design of computational algorithms for transient/dynamic applications", *Archives Comput. Methods Eng.*, **7**(2), 67-290. https://doi.org/10.1007/BF02736209.
Wen, W.B., Jian, K.L., and Luo, S.M. (1980), "An explicit time integration method for structural dynamics using septuple B-spline functions", *J. Numeric. Method. Eng.*, **97**(9), 629-657. https://doi.org/10.1002/nme.4599.
Wood, W.L., Bossak, M. and Zienkiewicz, O.C. (1980), "An alpha modification of Newmark's method", *J. Numeric. Method. Eng.*, **15**(10), 1562-1566. https://doi.org/10.1002/nme.1620151011.
Yin, S.H. (2013), "A new explicit time integration method for structural dynamics", *J. Struct. Stability Dynam.*, **13**(3), https://doi.org/10.1142/S021945541250068X.

CC